Supplementary information

Ambipolar to anti-ambipolar light induced transition in WSe_2-based FETs

Kimberly Intonti[1,2,*], Adolfo Mazzotti[1], Aniello Pelella[1], Filippo Giubileo[2], Nadia Martucciello[2], Stephen O'Sullivan [3], Vilas Patil[3], Paul K. Hurley[3,4], Lida Ansari[3], Farzan Gity[3], and Antonio Di Bartolomeo[1,*]

[1]*Department of Physics "E. R. Caianiello", University of Salerno, via Giovanni Paolo II, Fisciano, Salerno, 84084, Italy*

[2]*CNR-SPIN Salerno, via Giovanni Paolo II, Fisciano, 84084, Italy*

[3]*Tyndall National Institute, University College Cork, Lee Maltings, Dyke Parade, Cork, T12 R5CP, Ireland*

[4]*School of Chemistry, University College Cork, Cork, Ireland*

**Corresponding authors: kintonti@unisa.it, adibartolomeo@unisa.it*

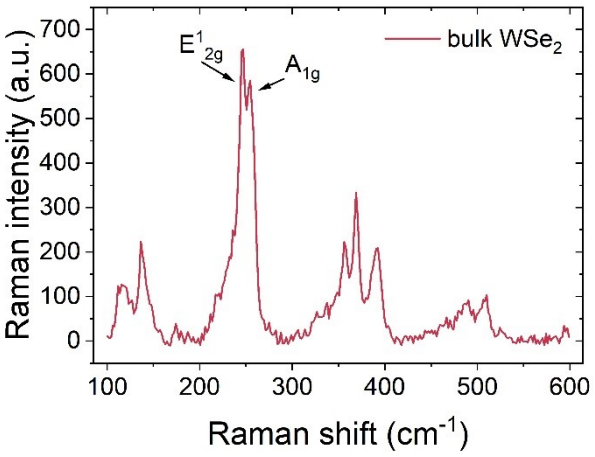

Figure S.1: Raman spectrum acquired on a WSe_2 flake subjected to the same fabrication process as the investigated device, obtained with a 70 mW 532 nm laser.

The Raman spectrum acquired on WSe_2-based devices fabricated through the same process as our investigated device shows clear signatures of bulk multilayer WSe_2. The two dominant peaks, fitted at approximately 247 cm^{-1} and 256 cm^{-1} correspond to the E^1_{2g} and A_{1g} modes, respectively, which are first-order Raman-active phonons [1]. In the literature, these peaks are often closely overlapped, giving a prominent peak at 250 cm^{-1}. A small peak near 176 cm^{-1} can be identified with the E_g mode. Additional features in the 300–400 cm^{-1} range can be identified as two-phonon modes from second-order Raman processes and interlayer modes typical of bulk WSe_2[2]."

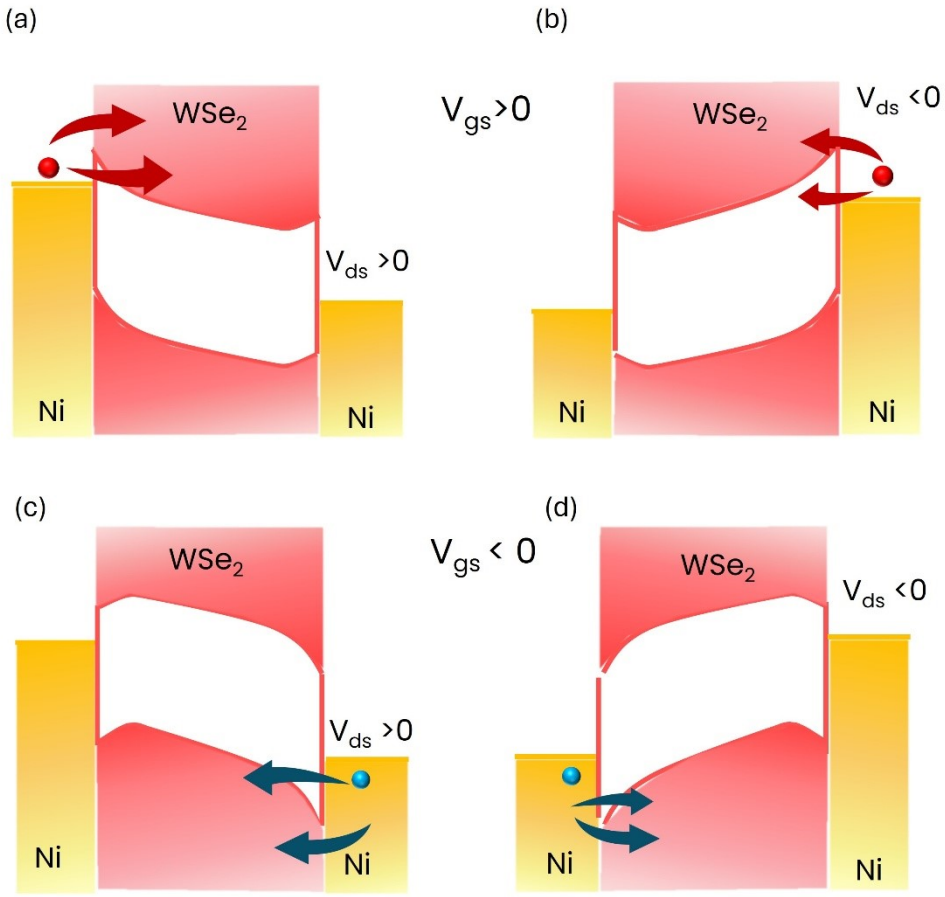

Figure S.2: Band diagrams illustrating the impact of Schottky barrier asymmetry on charge injection. (a) Positive drain bias favors electron injection more effectively than (b) negative drain bias. Similarly, (c) positive drain bias is more favorable for hole injection compared to (d) negative drain bias.

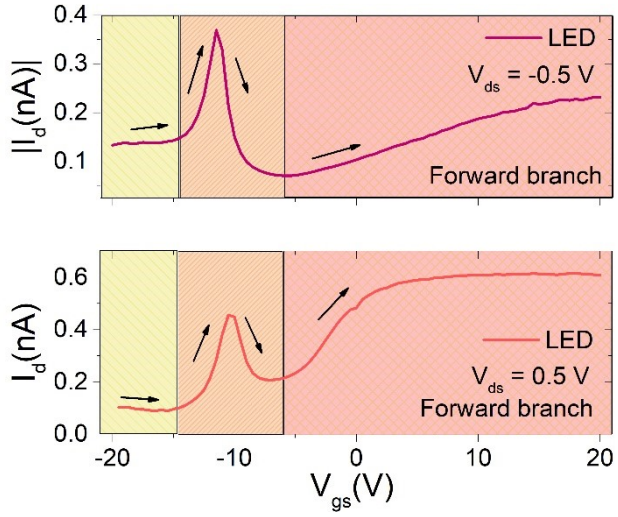

Figure S.3: Identification of three current levels in the forward branch of the transfer curves at V_{ds} = -0.5 (top) and 0.5 V (bottom) under LED light.

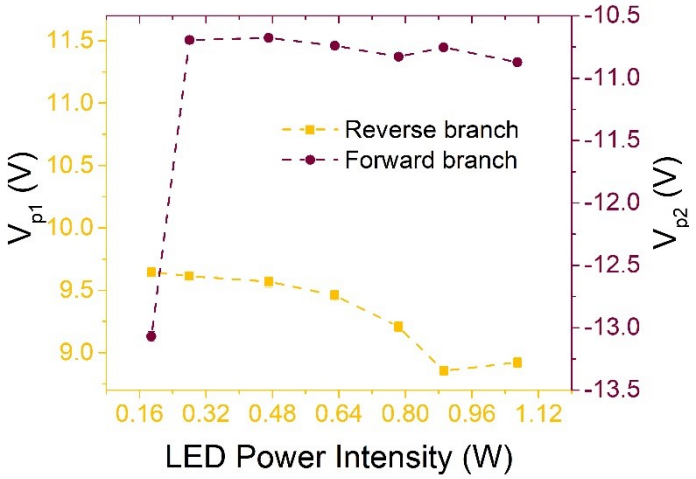

Figure S.4: Voltage bias at which the peak occurs as a function of the LED power intensity on the reverse (left) and forward (right) branch, respectively.

Table S.1: Comparison of the main figures of merit of anti-ambipolar devices

Work	Device structure	Material	Operating condition	Vp	PVCR	ΔV_g
Yao et al[3]	p-n junction	MoTe2/MoS2	Dark	-20	<10	
Sun et al[4]	p-n junction	InSe/MoTe2	Dark	-20	10^3	60
Lv et al[5]	P-n junction	SnS/WSe2		5	10^2	30
	p-n junction	BP/ReS2	Dark	0.4	4.2-6.9	
Nourbakhsh et al [1]	p-n junction	WSe2/MoS2	Dark	20	10^3	20
Ii et al[6]	p-n junction	SnS2/WSe2	Dark	-10	200	20
Han et al[7]	**In plane homojunction**	**WSe2**	**Light**	**-2.5**	**29.3**	
Wang et al[8]	**Single-material FET**	**WSe2**	**Light (no signal in the dark)**	**-6**	**40**	**20**
Thakar et al[9]	**Multi-gate structure**	**WSe2**	**dark**	**0**	**10^2**	**4**
Liu et al[10]	Single material FET	MoS2	Dark, low temperature	-20	47	40
This work	**Single material FET**	**Wse2**	**Light (red laser)**	**-12**	**<10**	**5-7**

As shown in Table 1, most anti-ambipolar devices reported in the literature rely on p–n junction architectures. In these structures, the appropriate combination of materials and threshold voltages creates gate-bias windows in which both transistors are simultaneously on, separated by regions where at least one of the two is off. Such devices typically exhibit high PVCR values because they exploit the independent modulation of the two materials and operate over relatively large ΔV_g ranges, which makes the transition between states less abrupt. Anti-ambipolar behavior has also been observed in bulk MoS_2, but only at low temperature, due to the formation of a vertical barrier arising from the reduced electrostatic control of the back gate over the

upper layers of the material. WSe_2 is a frequently used material in these architectures, and anti-ambipolar transport has been reported under illumination in an in plane lateral homojunction or double gate structures. Our device, although characterized by a modest PVCR, exhibits a very narrow ΔV_g and enables a light-induced transition from ambipolar to anti-ambipolar behavior in a simpler FET structure. This is different from other demonstrations that required multi-gate configurations to independently tune the barrier profiles within the device.

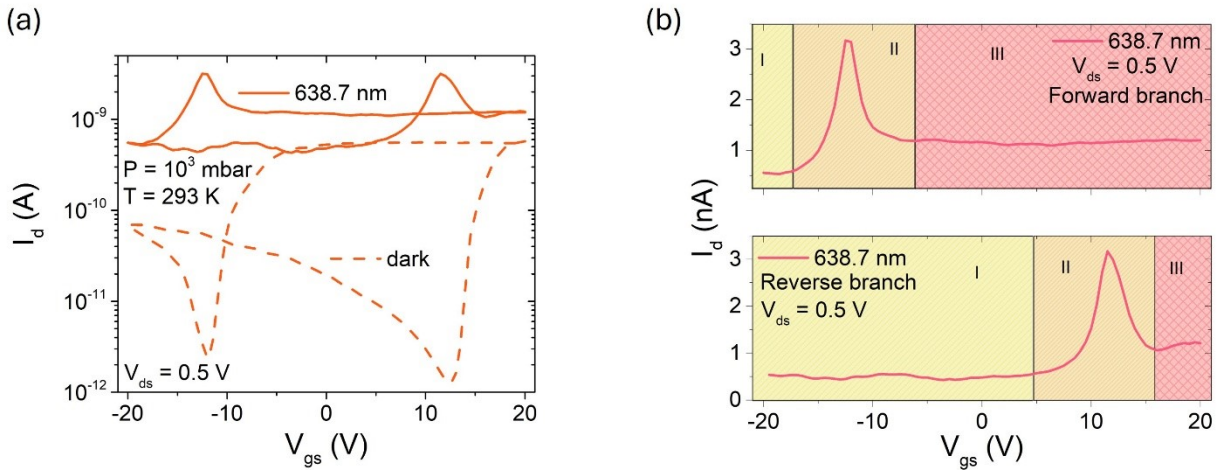

Figure S.5: (a) Comparison between the dark transfer curve at Vds=0.5 V and the transfer curves under illumination of a red laser. (b) identification of three operative regions in the forward and reverse branches of the transfer curve.

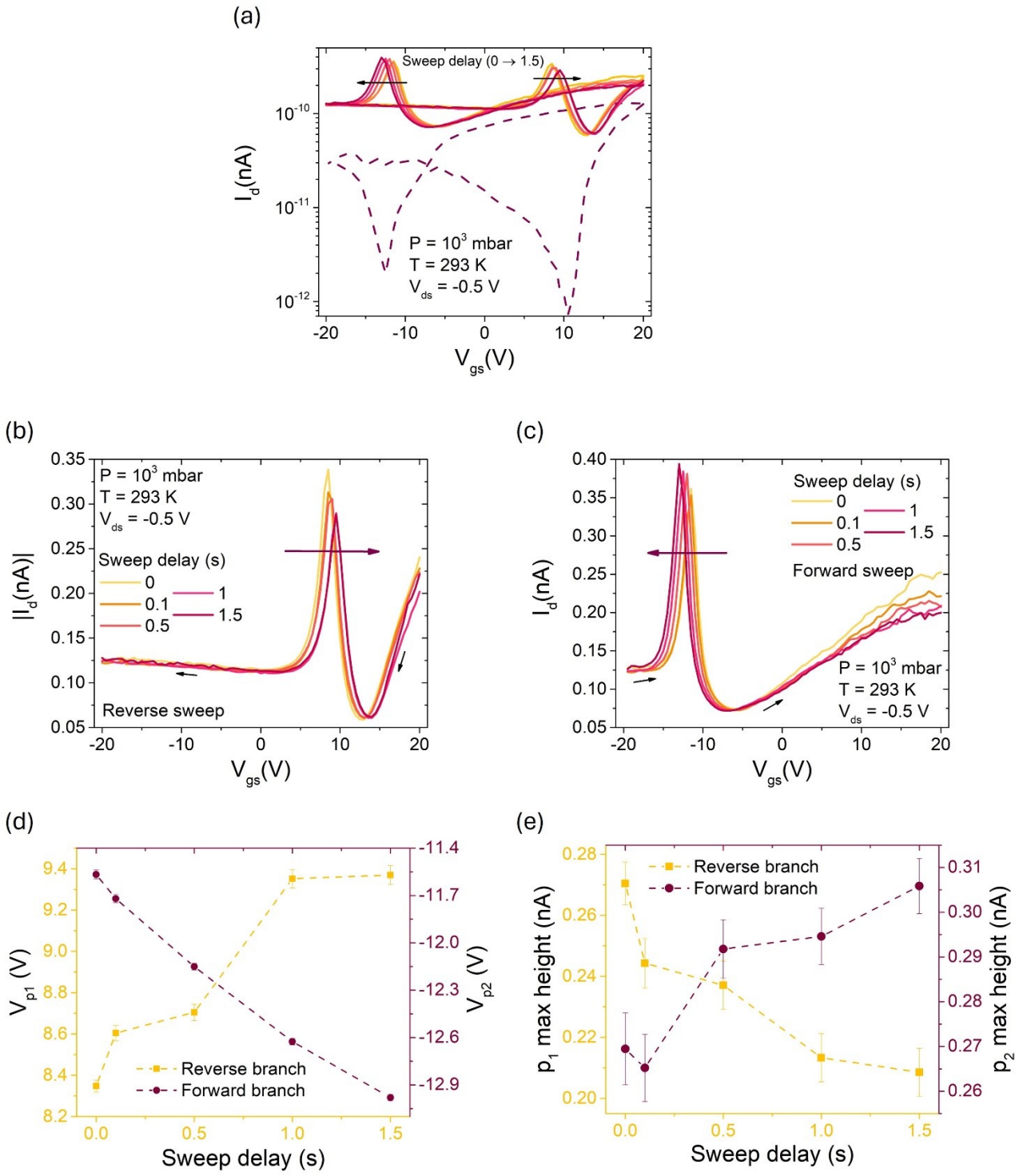

Figure S.6: (a) Comparison between the dark transfer curve at Vds=-0.5 V and the transfer curves under LED illumination obtained with different sweep delays in the measurement acquisition. Focus on (b) the reverse sweep and (c) the forward sweep of the transfer curve under LED illumination at different sweep delays. (d) Maximum points and (e) amplitudes of the peaks as a function of the sweep delay on the reverse branch (left) and the forward branch (right).

References

(1) Tonndorf, P.; Schmidt, R.; Böttger, P.; Zhang, X.; Börner, J.; Liebig, A.; Albrecht, M.; Kloc, C.; Gordan, O.; Zahn, D. R. T.; Vasconcellos, S. M. de; Bratschitsch, R. Photoluminescence Emission and Raman Response of Monolayer MoS_2, $MoSe_2$, and WSe_2. *Opt. Express* **2013**, *21* (4), 4908–4916. https://doi.org/10.1364/OE.21.004908.

(2) Blaga, C.; Álvarez, Á. L.; Balgarkashi, A.; Banerjee, M.; Morral, A. F. i; Dimitrievska, M. Unveiling the Complex Phonon Nature and Phonon Cascades in 1L to 5L WSe 2 Using Multiwavelength Excitation Raman Scattering. **2024**. https://doi.org/10.1039/D4NA00399C.

(3) Yao, H.; Wu, E.; Liu, J. Frequency Doubler Based on a Single MoTe2/MoS2 Anti-Ambipolar Heterostructure. *Appl. Phys. Lett.* **2020**, *117* (12), 123103. https://doi.org/10.1063/5.0018882.

(4) *Anti-ambipolar behavior and photovoltaic effect in p-MoTe2/n-InSe heterojunctions - Journal of Materials Chemistry C (RSC Publishing)*. https://pubs.rsc.org/en/content/articlelanding/2021/tc/d1tc02497c (accessed 2025-09-20).

(5) *Robust Anti-Ambipolar Behavior and Gate-Tunable Rectifying Effect in van der Waals p–n Junctions | ACS Applied Electronic Materials*. https://pubs.acs.org/doi/abs/10.1021/acsaelm.2c01120 (accessed 2025-11-21).

(6) *Anti-Ambipolar Field-Effect Transistors Based On Few-Layer 2D Transition Metal Dichalcogenides | ACS Applied Materials & Interfaces*. https://pubs.acs.org/doi/10.1021/acsami.6b02513 (accessed 2025-11-21).

(7) Han, H.; Zhang, B.; Zhang, Z.; Wang, Y.; Liu, C.; Singh, A. K.; Song, A.; Li, Y.; Jin, J.; Zhang, J. Light-Triggered Anti-Ambipolar Transistor Based on an In-Plane Lateral Homojunction. *Nano Lett.* **2024**, *24* (28), 8602–8608. https://doi.org/10.1021/acs.nanolett.4c01679.

(8) Wang, H.; Gao, W.; Wen, P.; Yu, H.; Huang, Y.; Yue, Q.; Wang, X.; Huo, N. Light-Regulated Anti-Ambipolar Transport with Multi-Logic States in Metal-WSe2-Metal Transistor. *Adv. Electron. Mater.* **2022**, *8* (12), 2200649. https://doi.org/10.1002/aelm.202200649.

(9) *Multi-Bit Analog Transmission Enabled by Electrostatically Reconfigurable Ambipolar and Anti-Ambipolar Transport | ACS Nano*. https://pubs.acs.org/doi/full/10.1021/acsnano.1c07032 (accessed 2025-11-21).

(10) *Vertical Charge Transport and Negative Transconductance in Multilayer Molybdenum Disulfides | Nano Letters*. https://pubs.acs.org/doi/10.1021/acs.nanolett.7b02161 (accessed 2025-11-21).